Rational design of $Cu_{2-x}Se$@(Co,Cu)Se_2 core-shell structure as bifunctional electrocatalyst for neutral-pH overall water splitting

Li Liu,*[a] Xiao Yang,[a] Yuanqing Zhao,[a] Bingbing Yao,[a] Yanhua Hou*[b] and Wensheng Fu*[a]

[a]Chongqing Key Laboratory of Green Synthesis and Applications, College of Chemistry, Chongqing Normal University, Chongqing 401331, China
[b]Chongqing Engineering Research Center of Pharmaceutical Sciences, Chongqing Medical and Pharmaceutical College, Chongqing 401331, China

Keywords: Neutral electrolyte, overall water splitting, bifunctional electrocatalysts, core-shell structure, synergistic effect.

*E-mail:liliu1208@163.com (L. Liu.)
*E-mail: fuwensheng@cqnu.edu.cn (W. Fu.)
*E-mail:hyh9785@163.com (Y. Hou)

Experimental section

Chemicals and Materials: Copper(II) Chloride Dihydrate ($CuCl_2·2H_2O$, AR**),** Sodium hydroxide (NaOH, AR), sodium thiosulfate pentahydrate ($NaS_2O_3·5H_2O$, AR**),** Sodium carbonate (Na_2CO_3, AR), ethyl alcohol (C_2H_5OH, AR), ethylene glycol ($(CH_2OH)_2$, AR) were purchased from Chengdu Kelong Chemical Co., Ltd. L-Ascorbic acid (Vc, 99.99%), Cobalt chloride hexahydrate ($CoCl_2·6H_2O$, 99%), Cobalt nitrate hexahydrate ($Co(NO_3)_2·6H_2O$, 99%), Selenium (Se**,** 99.99%) were provided by Shanghai Macklin Biochemical Co., Ltd. Polyvinylpyrrolidone ($(C_6H_9NO)_n$, Mw =40K) was obtained from Shanghai Yuanye Bio-Technology Co., Ltd. Ammonia solution ($NH_3·H_2O$, AR) was obtained from Chuandong chemical. The commercial RuO_2 was purchased from Sinopharm Group Chemical Reagent Co., Ltd. The commercial Pt/C was provided by Shanghai Aladdion Biochemical Technology Co., Ltd. In this experiment, all raw materials were not further purified, and deionized (DI) water (18.2 MΩ·cm) was used throughout the experiments.

Prepare of 1.0 M phosphate-buffered solution (pH 7): Firstly, 1mol/L KH_2PO_4 and 1mol/L K_2HPO_4 solution were prepared, respectively. Then, 610 mL 1mol/L KH_2PO_4 solution was mixed with 390 mL 1mol/L K_2HPO_4 solution. Finally, the pH meter was used to adjust the pH value (pH 7) of phosphate-buffered solution by adding strong acid or strong base solution.

Synthesis of Cu_2O Nanocube: The Cu_2O nanocube was synthesized by a familiar precipitation method. 0.171 g $CuCl_2·2H_2O$ and 0.556 g polyvinylpyrrolidone (PVP) were dissolved into 100 mL H_2O at 80 ℃ under the magnetic stirring, then 15 ml (2 M) NaOH was added into the mixture. After stirring for 30 min, 10 mL (0.6 M) Vc was slowly added into above solution. Following that, stirring for another 5 min, the obtained solution was aged in an oil bath at 80 °C for 2 h. The final product was centrifuged and washed several times with deionized water and absolute ethanol. After dried at 60 °C for 12 h, the Cu_2O nanocube was obtained.

Synthesis of Cu_2O@(Co,Cu)$(OH)_2$ intermediate: Cu_2O@(Co,Cu)$(OH)_2$ intermediate was prepared by a "coordinating-etching-precipitating" strategy. Firstly, 0.333 g PVP was dissolved in 5 mL anhydrous ethanol. Secondly, add 5 mL (1.0 mM) $CoCl_2·6H_2O$ to above solution with magnetic stirring. Then 50 mg as-prepared Cu_2O nanocube was poured into the above mixture. After stirring of 10 min, 5 mL (1 M) $NaS_2O_3·5H_2O$ solution was poured into the mixture. Then the mixture was stirred for another 10 min. Finally, the core-shell Cu_2O@(Co,Cu)$(OH)_2$ intermediate was collected by centrifugation, washed with DI water and anhydrous ethanol for several times, and then dried at 60 ℃ for 12 h.

Synthesis of $Cu_{2-x}Se$@(Co,Cu)Se_2 core-shell structure: 50 mg as-prepared Cu_2O@(Co,Cu)$(OH)_2$ intermediate and 50 mg selenium were placed downstream and upstream of the graphite boat, respectively. Then put graphite boat in a tube furnace. The furnace was heated to 500 ℃ at a heating rate of 5 ℃/min under a N_2 atmosphere and kept at 500 ℃ for 30 min. After natural cooling, the $Cu_{2-x}Se$@(Co,Cu)Se_2 core-shell structure was obtained.

Synthesis of $Cu_{2-x}Se$: In a typical procedure, 50 mg as-prepared Cu_2O nanocube and 50 mg

selenium were placed downstream and upstream of the graphite boat, respectively. Then put graphite boat in a tube furnace. After calcined the graphite boat at 500 ℃ for 30 min under a N_2 atmosphere, the $Cu_{2-x}Se$ was obtained.

Synthesis of $CoSe_2$: The $CoSe_2$ as contrast material was synthesized in two steps by general hydrothermal strategy and thermal decomposition. Firstly, add 12.5 mL Ammonia solution (AR) into 12.5 mL ethylene glycol (AR) to form a transparent solution. After stirring of 5 min, 5 mL (1M) Na_2CO_3 was poured into the above mixture. Subsequently, 5 mL (1M) $Co(NO_3)_2 \cdot 6H_2O$ was poured into in the admixture. After stirring for 20 min, the resulting uniform solution was maintained for 17 h at 170 ℃ in a 50 mL Teflon-lined autoclave. The product was washed with water and absolute ethanol several times. After dried for 12 h at 60 ℃, 50 mg as-obtained precursor was heated at 800 ℃ for 2 hours. When naturally cooled to room temperature, 200 mg selenium was quickly mixed in the graphite boat. After the graphite boat was heated at 400 ℃ for 30 min under a N_2 atmosphere, the $CoSe_2$ was obtained.

Characterization: The powder X-ray diffractometer (Lab XRD-6100, Cu Kα radiation (λ = 1.54184 Å)), Raman spectrometer equipped with argon (532 nm) laser in the wavenumber of 100-2000 cm^{-1} (Horiba LabRAM HR Evolution) and X-ray photoelectron spectrometer (ESCALAB250), Brunauer-Emmett-Teller surface area analyzer (BET, 3H-2000PS1), Scanning Electron Microscope (JEOL JSM-7800F) and Transmission Electron Microsphere (ThermoFisher Scientific, Talos F200s) were carried out to test the pure phase, component, valence states, surface area, morphology and structural features of as-prepared samples.

Electrochemical characterization: For the preparation of working electrode, 10 mg the as-obtained catalyst was well-dispersed in diluted Nafion alcohol solution consisting of 50 μL Nafion and 450 μL ethanol, followed by ultrasound for at least 30 min. Then, 10 μL the catalyst ink was dropped onto the glass carbon electrode (GCE, 6 mm in diameter) as working electrode for HER and OER. Electrochemical measurements were taken on a CHI660E electrochemistry workstation at room temperature using a typical three-electron system in 1.0 M phosphate-buffered solution (PBS). The catalyst on GCE was used as the working electrode, graphite rod and Ag/AgCl (in KCl saturated) acted as the counter electrode and reference electrode, respectively. All the potentials reported in this work were normalized against that of the reversible hydrogen electrode (RHE) using equation: $E_{RHE} = E_{Ag/AgCl} + 0.059pH + 0.197$. Before HER and OER tests, the electrolyte was continuously degassed by bubbling pure H_2 and O_2 for at least 30 min to acquire gas saturation, respectively. And before recording the test results, the cyclic voltammetry (CV) was firstly measured for at least 10 cycles for the purpose of achieving the stable state. The linear sweep voltammogram (LSV) curves were measured at 2 mV/s with an *iR* corrected. The voltage scope of HER and OER measurement is -1~-0.6 V and 0.6~1.2 V, respectively. The Tafel plots were derived from the polarization curves as |potential| vs.|log *j*|. Then, the Tafel slope (*b*) can be acquire by fitting the linear portion of Tafel plots to the Tafel equation ($\eta = b \log(j) + a$). To

estimate the electrochemically effective surface area (ECSA), the electrochemical double-layer capacitance (C_{dl}) was determined from the cyclic voltammetry (CV) curves measured in a non–faradic potential range (1.25~1.35 V vs RHE) with different scan rates ranging from 10~50 mV/s. The HER and OER durability were determined by the chronopotentiometric measurements at the current density of 10 and -10 mA/cm^2, respectively, as well as the cyclic voltammetry (CV) for 2000 cycles. Electrochemical impedance spectroscopy (EIS) was obtained by applying an AC voltage with 5 mV amplitude in the frequency region of 10^{-2}-10^5 Hz at open circuit voltage. And the Zview version 3.2c-software was used to parse the impedance data for OER and HER. For overall water splitting electrolysis, the catalyst ink was uniformly overlaid on carbon cloth (CC) with a cover area of 1cm^2 as working electrode. The loading mass of tested samples was controlled at 1± 0.1 mg/cm^2 as much as possible. A two-electrode configuration was assembled for electrochemical test, where as-prepared catalyst was used as both cathode and anode. For comparison, the two-electrode devices with commercial Pt/C and RuO_2 onto CC as the cathode and anode were also prepared. The LSV curves were performed in 1.0 M PBS at a scan rate of 2 mV/s. The long-term durability was tested by the chronopotentiometric measurement at the current density of 10 mA/cm^2 for 30h. All the potential in the paper, if not specified was recorded relative to the RHE and the current density was normalized to the geometrical surface area.

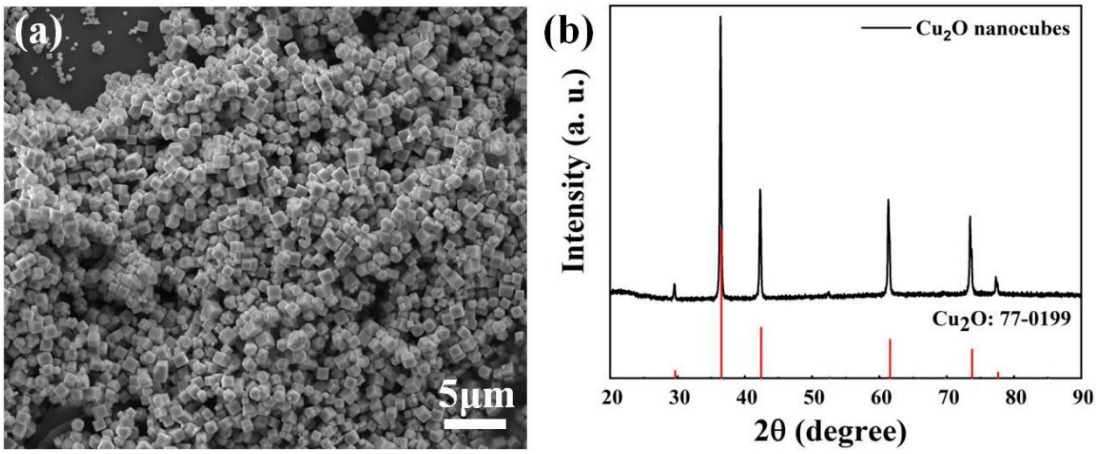

Figure S1. (a) SEM image of Cu_2O nanocubes on a large scale. (b) XRD pattern of Cu_2O nanocubes.

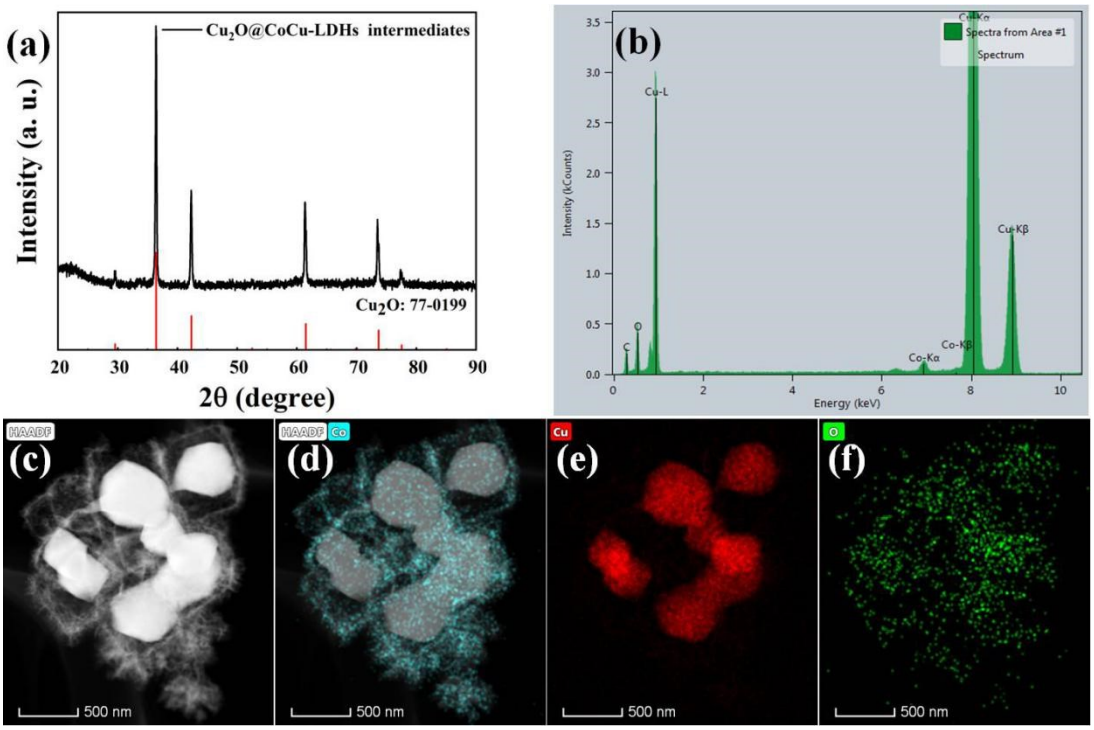

Figure S2. (a) XRD pattern, (b) EDX spectrum, (c) HAADF-STEM image and (d-f) EDX elemental mapping images of Cu_2O@$(Co,Cu)(OH)_2$ intermediates.

Figure S2a displays the XRD pattern of Cu_2O@$(Co,Cu)(OH)_2$ intermediates, which only exhibits the diffraction peaks of internal Cu_2O core (JCPDS No. 77-0199) without the diffraction peaks of $(Co,Cu)(OH)_2$ shell. This result implies the amorphous $(Co,Cu)(OH)_2$ phase. However, EDX spectrum in Figure S2b demonstrates that the Cu_2O@$(Co,Cu)(OH)_2$ intermediate contains Cu, Co, O and C elements, wherein C element comes from air. In addition, HAADF-STEM image (Figure S2c) explicitly proves the unique core-shell structure, in which ultrathin $(Co,Cu)(OH)_2$ nanosheets constitute the shell structure and Cu_2O nanocube gradually contracts to form a core. The fact is also verified by the elemental mapping images in Figure S2d-f.

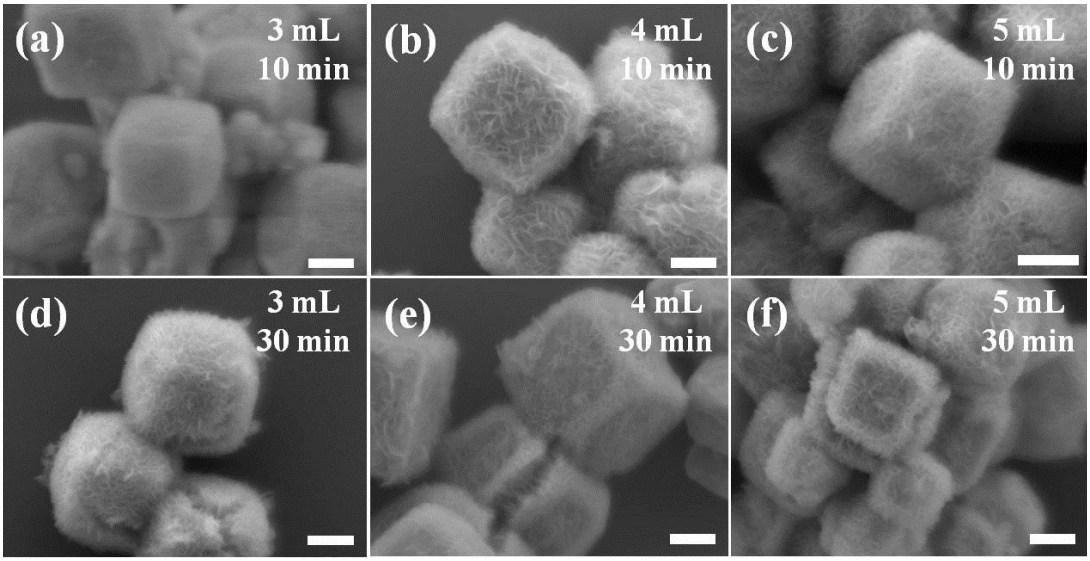

Figure S3. (a-f) The SEM images of Cu_2O@$(Co,Cu)(OH)_2$ intermediate with different dosages of 1M $Na_2S_2O_3$ and different reaction time. The scale bar is 500 nm.

Figure S3 displays that the $(Co,Cu)(OH)_2$ nanosheets on the surface gradually become lush with the increase of the dosage of $Na_2S_2O_3$, while with the extension of reaction time, the thickness of sheet-like shell increases, meanwhile, the internal Cu_2O core continuously dissolves forming a unstable hollow-structure instead of a core-shell structure. It can be seen that the optimal experimental condition is 5 mL 1M $Na_2S_2O_3$ with the reaction time of 10 min.

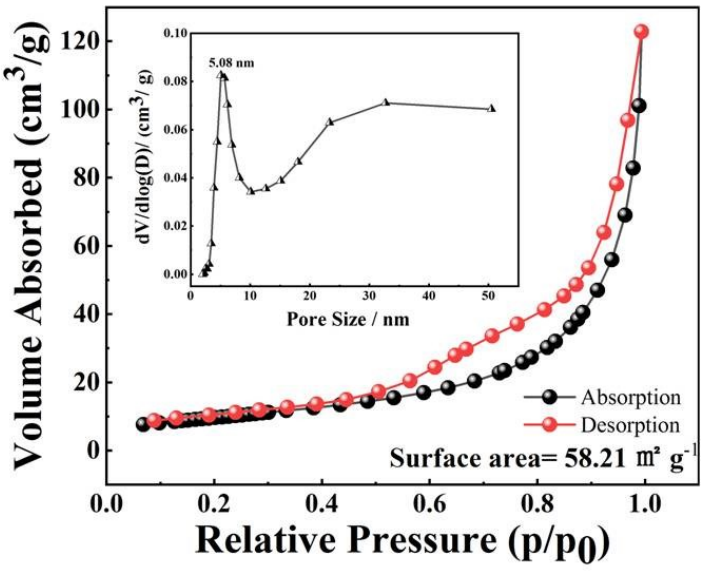

Figure S4. Nitrogen adsorption-desorption isotherms and the corresponding pore size distribution (inset) of $Cu_{2-x}Se$@$(Co,Cu)Se_2$ core-shell structures.

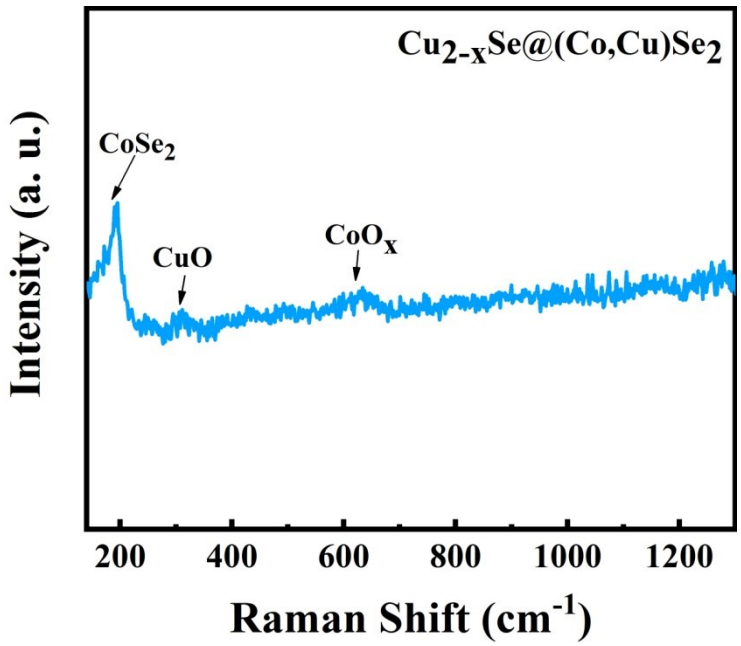

Figure S5. Raman spectrum of $Cu_{2-x}Se@(Co,Cu)Se_2$ core-shell structures.

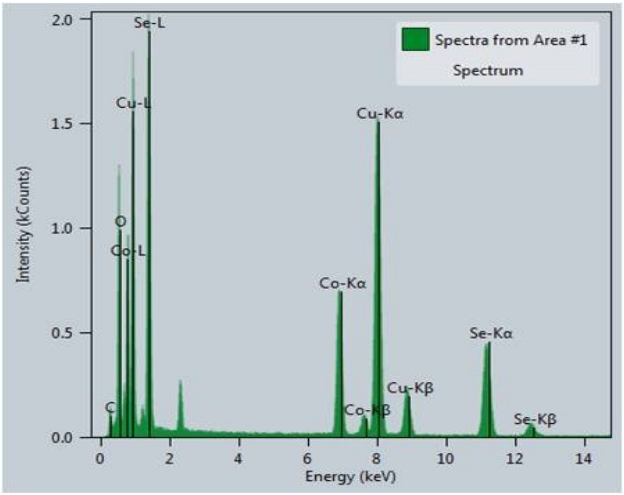

Figure S6. EDX spectrum of $Cu_{2-x}Se@(Co,Cu)Se_2$ core-shell structures.

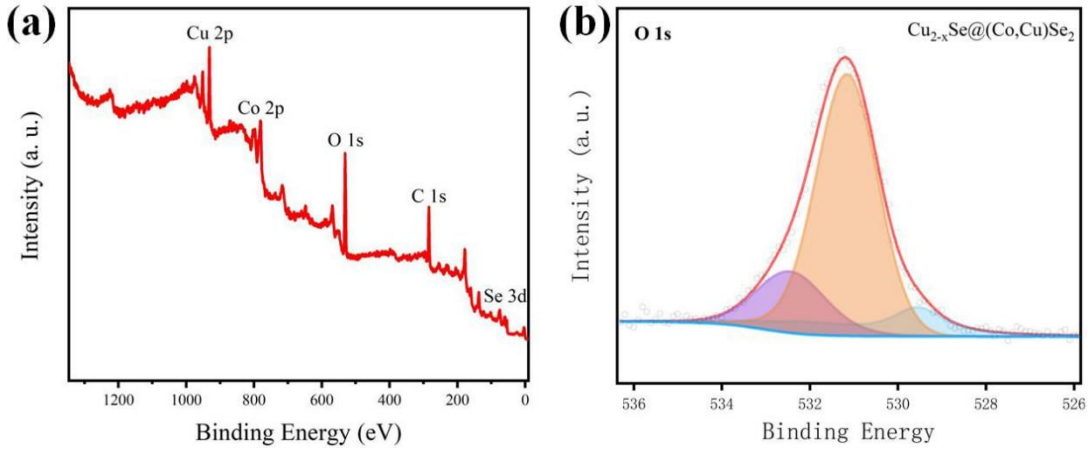

Figure S7. (a) XPS spectrum of $Cu_{2-x}Se@(Co,Cu)Se_2$ core-shell structures, (b) High-resolution XPS spectra of O1s for $Cu_{2-x}Se@(Co,Cu)Se_2$ core-shell structures.

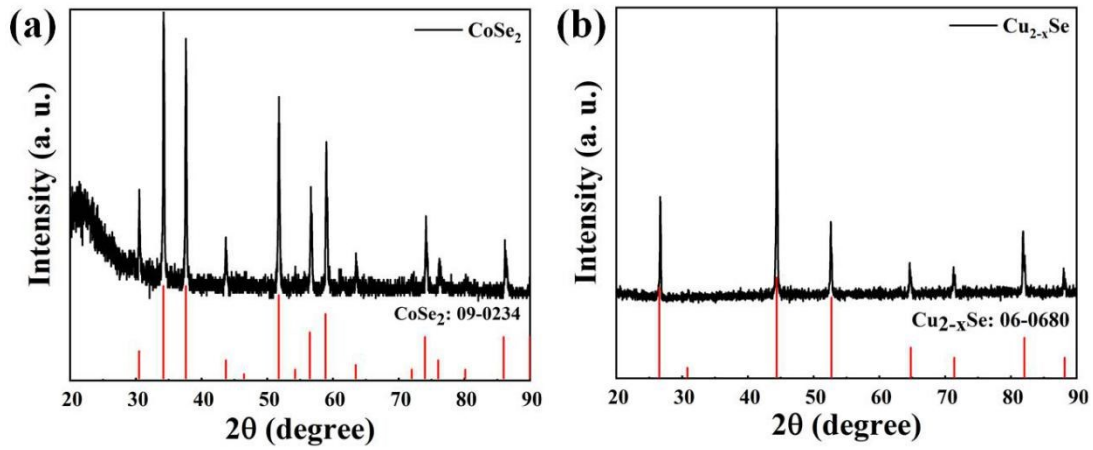

Figure S8. The XRD patterns of (a) $CoSe_2$ and (b) $Cu_{2-x}Se$.

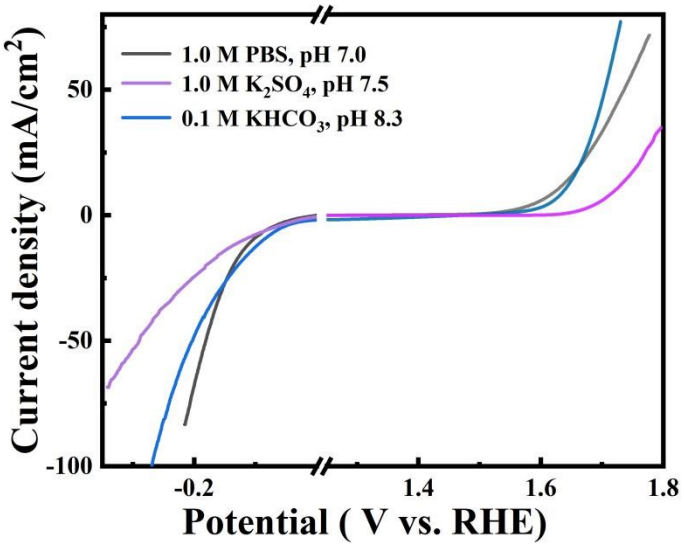

Figure S9. The linear sweep voltammetry (LSV) curves of $Cu_{2-x}Se$@(Co,Cu)Se_2 catalyst for HER and OER in several neutral and near-neutral electrolyte, such as phosphate buffer solution (1.0 M PBS, pH 7), K_2SO_4 solution (1.0 M, pH 7.5) and $KHCO_3$ solution (0.1 M, pH 8.3).

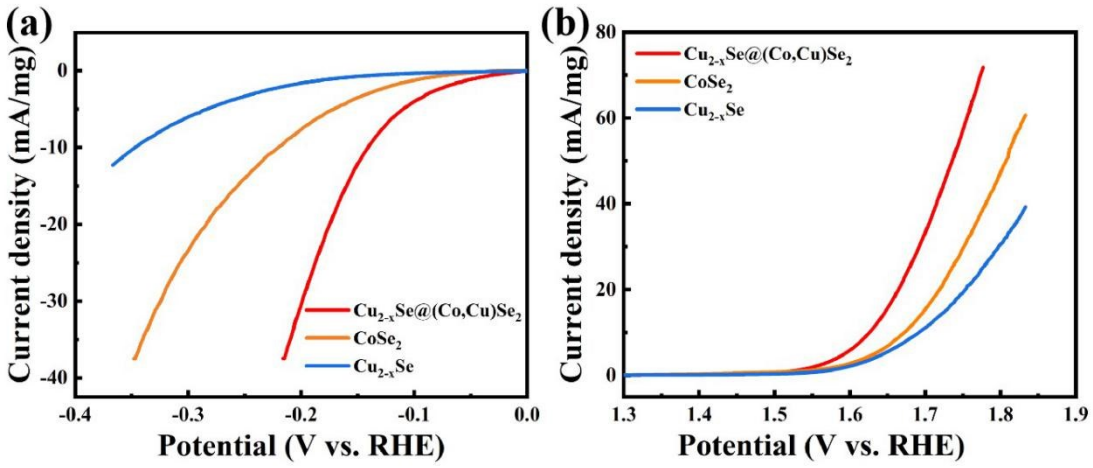

Figure S10. The mass activity of $Cu_{2-x}Se@(Co,Cu)Se_2$, $CoSe_2$, $Cu_{2-x}Se$ catalysts for (a) HER process and (b) OER process. The mass loading is about 0.2 mg.

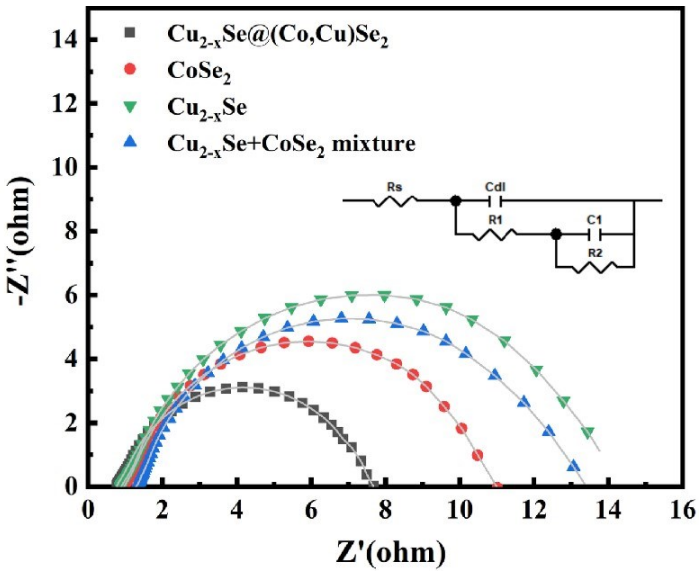

Figure S11. Nyquist plots of $Cu_{2-x}Se@(Co,Cu)Se_2$, $CoSe_2$, $Cu_{2-x}Se$ and $Cu_{2-x}Se+CoSe_2$ mixture for HER test. The scattered symbols represent the experimental results and the solid lines are simulation fitted results. The inset demonstrates the equivalent circuit for the simulation.

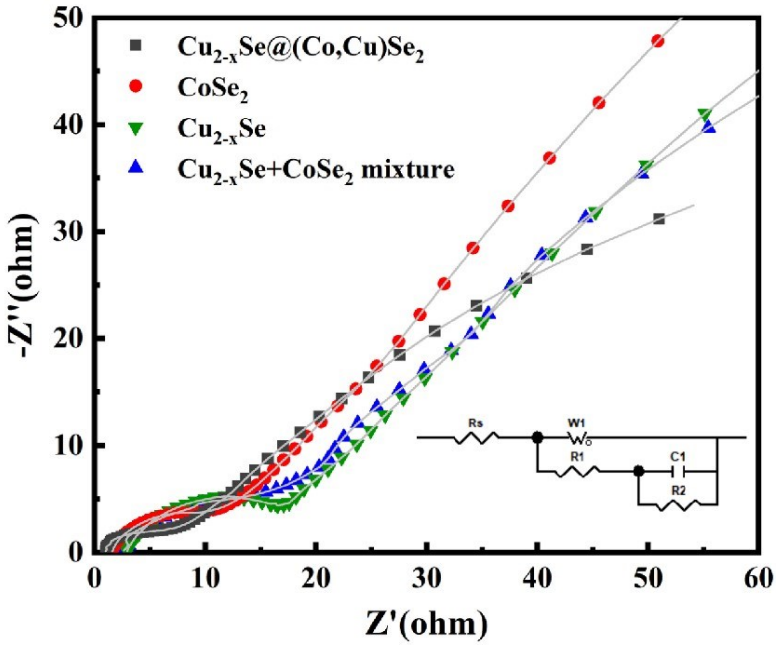

Figure S12. Nyquist plots of $Cu_{2-x}Se@(Co,Cu)Se_2$, $CoSe_2$, $Cu_{2-x}Se$ and $Cu_{2-x}Se+CoSe_2$ mixture for OER test. The scattered symbols represent the experimental results and the solid lines are simulation fitted results. The inset demonstrates the equivalent circuit for the simulation.

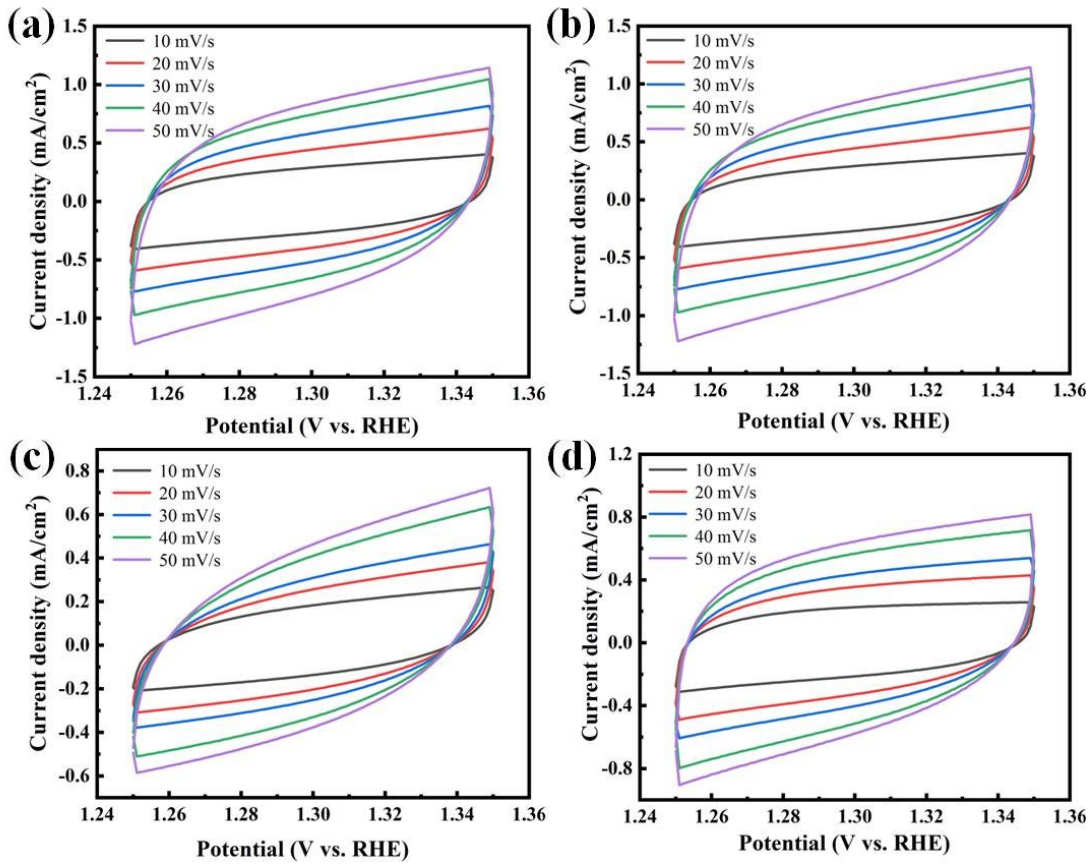

Figure S13. CV curves of (a) $Cu_{2-x}Se$@(Co,Cu)Se_2, (b) $CoSe_2$, (c) $Cu_{2-x}Se$ and (d) $Cu_{2-x}Se$+$CoSe_2$ mixture in the non-faradic current range at scan rates of 10~50 mV/s.

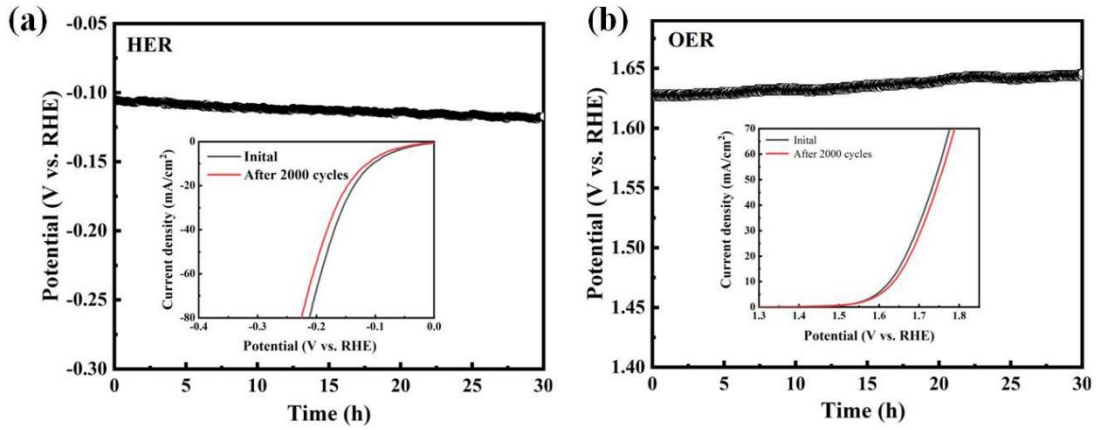

Figure S14. Long-term stability measurements of $Cu_{2-x}Se@(Co,Cu)Se_2$ at (a) -10 mA/cm^2 for HER and (b) 10 mA/cm^2 for OER. The inset is the corresponding CV curves of HER and OER, respectively, for 1st and 2000th cycles at a scan rate of 2 mV/s in 1.0 M PBS media.

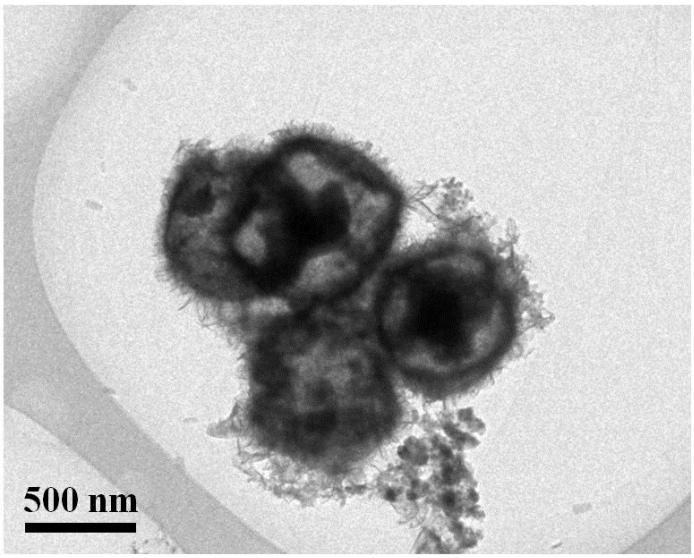

Figure S15. The low-magnification TEM image of $Cu_{2-x}Se$@(Co,Cu)Se_2 core-shell structures after OER measurements.

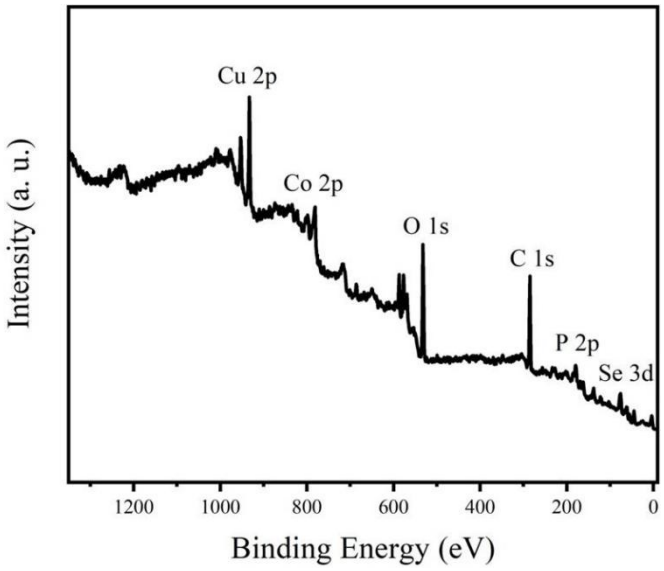

Figure S16. XPS spectrum of $Cu_{2-x}Se@(Co,Cu)Se_2$ core-shell structures after OER tests.

Table S1. The atomic concentration of C, O, Co, Cu and Se elements in $Cu_{2-x}Se@(Co,Cu)Se_2$ core-shell structure.

	Element	App	Intensity	Weight%	Weight%	Atomic%
Materials		Conc	Corrn.		Sigma	
$Cu_{2-x}Se@(Co,Cu)Se_2$ core-shell structure	C K	0.16	0.0262	1.73	0.12	2.94
	O K	1.12	0.1837	10.56	0.09	11.67
	Cu K	7.45	1.05	20.53	0.94	23.66
	Co K	2.11	0.7913	11.87	0.74	4.64
	Se K	2.58	0.6122	55.31	4.83	57.09
	Totals			100.00		

Table S2. The simulated R_{ct} values of $Cu_{2-x}Se@(Co,Cu)Se_2$, $CoSe_2$, $Cu_{2-x}Se$ and $Cu_{2-x}Se+CoSe_2$ catalysts for HER test.

Catalysts	$Cu_{2-x}Se@(Co,Cu)Se_2$	Bare $CoSe_2$	Bare $Cu_{2-x}Se$	$Cu_{2-x}Se+CoSe_2$ mixture
R_{ct} (Ω)	6.104	10.005	13.926	13.188

Table S3. The simulated R_{ct} values of $Cu_{2-x}Se@(Co,Cu)Se_2$, $CoSe_2$, $Cu_{2-x}Se$ and $Cu_{2-x}Se+CoSe_2$ catalysts for OER test.

Catalysts	$Cu_{2-x}Se@(Co,Cu)Se_2$	Bare $CoSe_2$	Bare $Cu_{2-x}Se$	$Cu_{2-x}Se+CoSe_2$ mixture
R_{ct} (Ω)	7.037	15.421	18.414	27.895

Table S4. Comparison of HER catalytic performance in neutral-pH media with other non-noble metal catalysts on recently available literatures.

Catalyst	Electrolyte (PBS)	Tafel slope (mV/dec)	Overpotential (η_{10}) (mV)	Reference
$Ni_{0.1}Co_{0.9}P$	1 M	103	125	[1]
S-$NiFe_2O_4$/NF	1 M	81.3	197	[2]
$Ni_{0.89}Co_{0.11}Se_2$	1 M	78	88	[3]
Cu-CoP NAs/CP	1 M	83.5	81	[4]
Ni-Co-P-H	0.5 M	84	157	[5]
Co/CoP-5	1 M	72.3	138	[6]
Karst NF	1 M	99	110	[7]
Cu_3N-Cu_3P/NPSCNWs@NF	1 M	124	109	[8]
CoP/CC	1 M	129	106	[9]
PD-CoP UNSs/CC	1 M	101	90	[10]
SiO_2/PPy NTs-CFs	1 M	100.2	183	[11]
np-Co_9S_8	1 M	118	264	[12]
β-Cu_2S/CF	1 M	125.5	190	[13]
CoO/$CoSe_2$	0.5M	131	337	[14]
1%CoS2-9% CuS	0.5M	90	89	[15]
Co_9S_8/Ni_3S_2/NF	1 M	82	330	[16]
$Fe_{10}Co_{40}Ni_{40}P$	1 M	132	300	[17]
$Ni(S_{0.5}Se_{0.5})_2$	1 M	81	124	[18]
FeP/$Co_3(PO_4)_2$	1 M	81	117	[19]
CoP/Co_2P@NC-2	1M	---	498	[20]
RuCo@CDs	1M	67	171	[21]
$Cu_{2-x}Se$@$(Co,Cu)Se_2$	**1 M**	**81**	**106**	**This work**

Table S5. Comparison of OER catalytic performance in neutral-pH media with other non-noble metal catalysts on recently available literatures.

Catalyst	Electrolyte (PBS)	Tafel slope (mV/dec)	Overpotential (η_{10}) (mV)	Reference
$Ni_{0.1}Co_{0.9}P$	1 M	133	570	22
RhCo-ANAs	1 M	139	310	23
S-$NiFe_2O_4$/NF	1 M	118.1	494	2
CoO_xH_y/CC	0.1 M	121	430@38mA/cm^2	24
FeNi-P/NF-A	0.1 M	136	429	25
$Cu_{0.08}Co_{0.92}P$/CP	1 M	83.5	411	4
Karst NF	1 M	249	432	7
CoO/$CoSe_2$/Ti	0.5 M	198	510	14
CoO/Co_4N	1 M	83	398	26
Co_9S_8/Ni_3S_2/NF	1 M	226	495	16
Co-Pi NA/Ti	0.1 M	187	380	27
Co_3S_4/AC	1 M	170	360	28
$Fe_{10}Co_{40}Ni_{40}P$	1 M	246	466	17
Ni_3Se_4@Ni foam	1 M	116	480	18
$Ni(S_{0.5}Se_{0.5})_2$	1 M	94	501	29
FeP/$Co_3(PO_4)_2$	1 M	301	504	19
RuCo@CDs	1 M	147.4	410	21
$Cu_{2-x}Se$@(Co,Cu)Se_2	**1 M**	**102**	**396**	**This work**

Table S6. Performance comparison of overall water splitting with other systems in neutral-pH electrolyte.

Catalyst	Electrolyte (PBS)	Cell voltage at 10 mA cm^2 (V)	Reference
$Ni_{0.1}Co_{0.9}P$	1 M	1.89	[1]
RhCo-ANAs/CF	1 M	1.58	[23]
S-$NiFe_2O_4$/NF	1 M	1.95	[2]
Cu-CoP NAs/CP	1 M	1.72	[4]
A- P- $CoMoO_4$‖ NiFeDH	1 M	1.74	[30]
Karst NF	1 M	1.88	[7]
Cu_3N-Cu_3P/NPSCNWs@NF	1 M	1.54	[8]
np-Co_9S_4P	1 M	1.67	[12]
CoO/$CoSe_2$-Ti	0.5 M	2.18	[14]
CoO/Co_4N	1 M	1.79	[26]
MoS_2/Co_9S_8/Ni_3S_2/Ni	1 M	1.80	[16]
Co-Pi NA/Ti	1 M	1.82	[27]
$Fe_xCo_yNi_zP$	1 M	1.57	[17]
$Ni(S_{0.5}Se_{0.5})_2$	1 M	1.87	[29]
FeP/$Co_3(PO_4)_2$	1 M	1.82	[19]
RuCo@CDs	1 M	1.64	[21]
$Cu_{2-x}Se$@(Co,Cu)Se_2	**1M**	**1.73**	**This work**

Notes and Reference

1. R. Wu, B. Xiao, Q. Gao, Y.-R. Zheng, X.-S. Zheng, J.-F. Zhu, M.-R. Gao and S.-H. Yu, *Angew. Chem. Int. Ed.*, 2018, **57**, 15445-15449.
2. J. Liu, D. Zhu, T. Ling, A. Vasileff and S.-Z. Qiao, *Nano Energy*, 2017, **40**, 264-273.
3. B. Liu, Y.-F. Zhao, H.-Q. Peng, Z.-Y. Zhang, C.-K. Sit, M.-F. Yuen, T.-R. Zhang, C.-S. Lee and W.-J. Zhang, *Adv. Mater.*, 2017, **29**, 1606521.
4. L. Yan, B. Zhang, J. Zhu, Y. Li, P. Tsiakaras and P. Kang Shen, *Appl. Catal. B: Environ.*, 2020, **265**, 118555.
5. X. Liu, S. Deng, D. Xiao, M. Gong, J. Liang, T. Zhao, T. Shen and D. Wang, *ACS Appl. Mater. Interfaces*, 2019, **11**, 42233-42242.
6. Z.-H. Xue, H. Su, Q.-Y. Yu, B. Zhang, H.-H. Wang, X.-H. Li and J.-S. Chen, *Adv. Energy Mater.*, 2017, **7**, 1602355.
7. X. Q. Gao, Y. D. Chen, T. Sun, J. M. Huang, W. Zhang, Q. Wang and R. Cao, *Energy Environ. Sci.*, 2020, **13**, 174-182.
8. Q. J. Wang, Z. Y. Zhang, X. Z. Zhao, J. W. Xiao, D. Manoj, F. F. Wei, F. Xiao, H. R. Wang and S. Wang, *Chemelectrochem*, 2020, **7**, 289-298.
9. J. Q. Tian, Q. Liu, A. M. Asiri and X. P. Sun, *J. Am. Chem. Soc.*, 2014, **136**, 7587-7590.
10. Y. L. Dang, J. K. He, T. L. Wu, L. P. Yu, P. Kerns, L. Y. Wen, J. Ouyang and S. L. Suib, *ACS Appl. Mater. Interfaces*, 2019, **11**, 29879-29887.
11. J.-X. Feng, H. Xu, S.-H. Ye, G. Ouyang, Y.-X. Tong and G.-R. Li, *Angew. Chem. Int. Ed.*, 2017, **56**, 8120-8124.
12. Y. W. Tan, M. Luo, P. Liu, C. Cheng, J. H. Han, K. Watanabe and M. W. Chen, *ACS Appl. Mater. Interfaces*, 2019, **11**, 3880-3888.
13. M. H. Fan, R. Q. Gao, Y. C. Zou, D. J. Wang, N. Bai, G. D. Li and X. X. Zou, *Electrochim. Acta*, 2016, **215**, 366-373.
14. K. D. Li, J. F. Zhang, R. Wu, Y. F. Yu and B. Zhang, *Adv. Sci.*, 2016, **3**, 1500426.
15. M. C. Li, Y. T. Qian, J. M. Du, H. R. Wu, L. Y. Zhang, G. Li, K. D. Li, W. M. Wang and D. J. Kang, *ACS Sustainable Chem. Eng.*, 2019, **7**, 14016-14022.
16. Y. Yang, H. Q. Yao, Z. H. Yu, S. M. Islam, H. Y. He, M. W. Yuan, Y. H. Yue, K. Xu, W. C. Hao, G. B. Sun, H. F. Li, S. L. Ma, P. Zapol and M. G. Kanatzidis, *J. Am. Chem. Soc.*, 2019, **141**, 10417-10430.
17. Z. Zhang, J. H. Hao, W. S. Yang and J. L. Tang, *RSC Adv.*, 2016, **6**, 9647-9655.
18. S. Anantharaj, J. Kennedy and S. Kundu, *ACS Appl. Mater. Interfaces*, 2017, **9**, 8714-8728.
19. H. X. Liu, X. Y. Peng, X. J. Liu, G. C. Qi and J. Luo, *Chemsuschem*, 2019, **12**, 1334-1341.
20. X. W. Lv, J. T. Ren, Y. S. Wang, Y. P. Liu and Z. Y. Yuan, *ACS Sustainable Chem. Eng.*, 2019, **7**, 8993-9001.
21. T. L. Feng, G. T. Yu, S. Y. Tao, S. J. Zhu, R. Q. Ku, R. Zhang, Q. S. Zeng, M. X. Yang, Y. X. Chen, W. H. Chen, W. Chen and B. Yang, *J. Mater. Chem. A*, 2020, **8**, 9638-9645.
22. R. Wu, B. Xiao, Q. Gao, Y. R. Zheng, X. S. Zheng, J. F. Zhu, M. R. Gao and S. H. Yu, *Angew. Chem., Int. Ed.*, 2018, **57**, 15445-15449.
23. Y. Zhao, J. Bai, X. R. Wu, P. Chen, P. J. Jin, H. C. Yao and Y. Chen, *J. Mater. Chem. A*, 2019, **7**, 16437-16446.
24. M. Q. Chen, Y. Y. Xie, J. X. Wu, H. F. Huang, J. Teng, D. W. Wang, Y. N. Fan, J. J. Jiang, H. P. Wang and C. Y. Su, *J. Mater. Chem. A*, 2019, **7**, 10217-10224.
25. B. W. Zhang, Y. H. Lui, L. Zhou, X. H. Tang and S. Hu, *J. Mater. Chem. A*, 2017, **5**, 13329-13335.
26. R. Q. Li, P. F. Hu, M. Miao, Y. L. Li, X. F. Jiang, Q. Wu, Z. Meng, Z. Hu, Y. Bando and X. B. Wang, *J. Mater. Chem. A*, 2018, **6**, 24767-24772.
27. L. S. Xie, R. Zhang, L. Cui, D. N. Liu, S. Hao, Y. J. Ma, G. Du, A. M. Asiri and X. P. Sun, *Angew. Chem. Int. Ed.*, 2017, **56**, 1064-1068.
28. M. Chauhan and S. Deka, *ACS Appl. Energy Mater.*, 2020, **3**, 977-986.
29. L. Y. Zeng, K. A. Sun, Y. J. Chen, Z. Liu, Y. J. Chen, Y. Pan, R. Y. Zhao, Y. Q. Liu and C. G. Liu, *J. Mater. Chem. A*, 2019, **7**, 16793-16802.

30. X. Cui, Y. Cui, M. L. Chen, R. Xiong, Y. C. Huang and X. W. Liu, *ACS Appl. Mater. Interfaces*, 2020, **12**, 30905-30914.